

NANO EXPRESS

Open Access

Nucleation and growth of primary nanostructures in SrTiO₃ homoepitaxy

Soo-hyon Phark^{1,2} and Young Jun Chang^{3*}

Abstract

SrTiO₃ nanoislands on SrTiO₃ (001) in a *diffusion-limited growth* regime were studied using *in situ* scanning tunneling microscopy (STM). The STM images revealed two characteristic features of nucleation stages. First, the minimum lateral size of the one-unit-cell (*uc*)-high SrTiO₃ islands was $4 \times 4 \text{ uc}^2$. Second, one-dimensional SrTiO₃ islands of a 4 uc width grew along the crystal symmetry directions. These observations suggest that $4 \times 4 \text{ uc}^2$ islands act as a minimum nucleation seed, and the addition of SrTiO₃ molecular species of the same width is the primary and dominant growth process in SrTiO₃ homoepitaxy. A close inspection of the surface of the substrate during the deposition process revealed possible connections between surface reconstruction and energetically favorable nucleation of SrTiO₃ islands.

Keywords: Island nucleation; Scanning tunneling microscopy; Perovskite homoepitaxy; Surface reconstruction

Background

Atomic-scale control over oxide surfaces and interfaces is one of the most important technological advances required to exploit the functionality of oxide materials. SrTiO₃ is one of the most widely studied oxide materials and has been the focus of research interest in the metal-insulator transition, [1] ferroelectricity [2,3], and superconductivity [4]. Recent advances in oxide film deposition techniques, including pulsed laser deposition (PLD) and molecular beam epitaxy, have enabled the formation of atomically flat surfaces, as well as controlled film-substrate interfaces. Perovskite films and interfaces grown on SrTiO₃ exhibit numerous interesting phenomena, including high-mobility quasi-two-dimensional electron gases [5-7], magnetism [8,9], and superconductivity [10,11]. Also, SrTiO₃ is a promising candidate for the study of the growth of nanostructures. Nanostructures grown on SrTiO₃ substrates have potential applications in the development of arrays of nanowires and quantum dots [12].

Despite the high crystalline quality of such perovskite films grown on SrTiO₃, microscopic observations of the nucleation of perovskite films during growth have not advanced significantly due to the structural complexity

and energetic instabilities arising from the volatility of oxygen [13,14]. Additionally, surface termination and reconstruction (RCs) are highly dependent on the oxygen partial pressure (P_{O_2}), as well as the temperature, which complicates any investigation of the mechanisms of film growth [15-17].

Scanning tunneling microscopy (STM) in the *diffusion-limited growth* regime allows the observation of the diffusion of single adatoms, and it has revealed the governing diffusion parameters, i.e., the surface diffusion barrier energy E_d and the attempt frequency ν_0 , for a number of metal films on metal substrates [18,19]. To apply the same methodology to the growth of perovskite oxide films, SrTiO₃ homoepitaxy provides a simple test case.

Here, we report STM studies of nucleation behavior during the growth of SrTiO₃ films on (2×1) reconstructed SrTiO₃ (001) surfaces. Using PLD growth with low coverage and growth temperatures, we realized *diffusion-limited growth* of SrTiO₃ films. The STM data revealed that the minimum lateral size of the SrTiO₃ nanostructures was approximately $4 \times 4 \text{ uc}^2$ and that such primary structures expand to form one-dimensional (1D) or two-dimensional (2D) islands as either the coverage or the growth temperature increased. High-resolution STM analysis provides insight into the

* Correspondence: yjchang@uos.ac.kr

³Department of Physics, University of Seoul, Seoul 130-743, Republic of Korea
Full list of author information is available at the end of the article

influence of surface RC and oxygen vacancies on the nucleation stage of island growth.

Methods

Nb (0.1%)-doped SrTiO₃ (001) single crystals (CrysTec GmbH) were used as substrates to obtain a sufficiently large electrical conductivity for the STM analysis. To exclude the effects of surface termination on the film growth, we removed the SrO-terminated fraction of the surface by treating the substrate in NH₄F-buffered HF solution [20] prior to placing the samples in the growth chamber. Experiments were carried out in a combined ultra-high vacuum (UHV) STM system (with a base pressure of $< 2 \times 10^{-10}$ Torr, Omicron VT-SPM) and custom-built PLD chamber (with a base pressure of $< 2 \times 10^{-9}$ Torr). Electrochemically etched tungsten tips were used for the STM measurements. Resistive heating in the UHV chamber was used to regulate the substrate temperature T_{sub} , which was monitored during the *in situ* surface preparation and SrTiO₃ deposition using an optical pyrometer with emissivity of 0.8. Thermal annealing of the substrate with $P_{\text{O}_2} = 1 \times 10^{-2}$ Torr at $T_{\text{sub}} = 900^\circ\text{C}$ was carried out for 30 min to provide an atomically flat surface with a well-ordered (2×1) RC

and one-unit-cell (*uc*)-high (0.3905 nm) steps, as determined using reflection high-energy electron diffraction (RHEED) and STM. Growth was initiated on such TiO₂-terminated surfaces [21–23] by ablating SrTiO₃ single crystal targets with $P_{\text{O}_2} = 1 \times 10^{-4}$ Torr using a KrF excimer laser ($\lambda = 248$ nm) with energy density of approximately 3 J/cm² at the target surface.

Results and discussion

Figure 1 shows STM topographic images for SrTiO₃ films that were 0.6-, 0.3-, and 0.1-monolayer (ML) thick grown at $T_{\text{sub}} = 580^\circ\text{C}$. The height profile across the surface reveals that the deposited layer is 1 *uc* high (i.e., approximately 0.4 nm), as shown in Figure 1d. When the surface coverage was greater than that of a critical coverage of approximately 0.5 ML, coalescence of islands occurred, and the film exhibited relatively homogeneous 2D growth patterns, as shown in Figure 1a, which were maintained until the coverage reached approximately 1 ML (not shown). However, the growth pattern was inhomogeneous in terms of both size and shape when the coverage was less than that required for coalescence (i.e., < 0.5 ML), as can be seen for the 0.3-ML film shown in Figure 1b. The STM image of the 0.1-ML sample shown

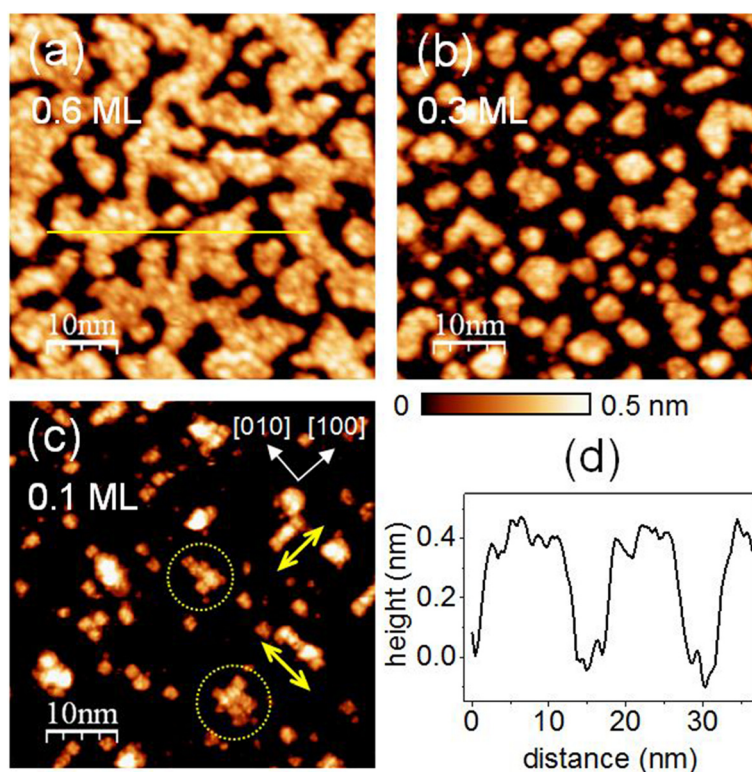


Figure 1 STM images for a coverage dependence of SrTiO₃ homoepitaxy. The $50 \times 50\text{-nm}^2$ STM images of (a) 0.6-ML, (b) 0.3-ML, and (c) 0.1-ML SrTiO₃ films grown on (2×1) reconstructed 0.1% Nb-doped SrTiO₃ (001) surfaces at $T_{\text{sub}} = 580^\circ\text{C}$. The crystallographic axes are shown by the yellow arrows in (c), and some larger islands are indicated by the dotted yellow circles. All STM images were obtained with $V_s = 2.5$ V and $I_{\text{set}} = 50$ pA. (d) The height profile along the yellow line in (a).

in Figure 1c reveals islands with a spatial extent of a few nanometers, which were less homogeneous with greater anisotropy than those in the 0.3-ML film. Some islands were elongated along the $\langle 100 \rangle$ crystal axes of SrTiO_3 . Larger islands appear to be produced by 2D aggregation of smaller square formations.

The observations in Figure 1 draw our attention to the use of high-resolution STM in homoepitaxy of SrTiO_3 in the *diffusion-limited growth* regime to obtain insight into the fundamental behavior of nucleation of the perovskite oxide islands. We carried out SrTiO_3 homoepitaxy with submonolayer coverage in a *diffusion-limited growth* regime to obtain small thermally stable SrTiO_3 islands. We inhibited island coalescence following nucleation by carrying out deposition at temperatures in the range $580 < T_{\text{sub}} < 620^\circ\text{C}$ to reduce thermal diffusion as low as possible [17,24,25] and maximized the island-island separation by forming films using a very low coverage during the PLD process. A large laser pulse interval of 1 min was used to allow sufficient time for the deposited species to form thermally equilibrated configurations following each laser ablation event. We confirmed that the samples were fully thermally relaxed by monitoring the recovery of the RHEED intensities following each laser pulse. We prepared three sets of samples, which were distinguished by the number of laser pulses such that each set was composed of two samples grown at $T_{\text{sub}} = 580^\circ\text{C}$ and 620°C .

Figure 2a and 2b show images of SrTiO_3 films following a single pulse (1-p) at $T_{\text{sub}} = 580^\circ\text{C}$ and 620°C , respectively. The images reveal the formation of SrTiO_3 islands of extremely small size, with a height of 1 *uc* (≈ 0.39 nm). At $T_{\text{sub}} = 580^\circ\text{C}$, most of the islands were square and uniform in size. The inset of Figure 2a shows a high-resolution STM image of the smallest SrTiO_3 island observed in this study. All four sides of the island were parallel to the directions of the crystallographic base vectors, i.e., $[100]$ and $[010]$. The length of each side was approximately 1.6 nm, corresponding to 4 *uc*; hence, we term such square islands $4 \times 4\text{-uc}^2$ SrTiO_3 . We observed larger islands that were rod-shaped at $T_{\text{sub}} = 620^\circ\text{C}$, as shown in Figure 2b. The longer side was several times the length of the shorter side and was parallel to the crystallographic axes; interestingly, the shorter side was 4-*uc*-long SrTiO_3 .

Figure 2c shows an STM image of a 2-p sample grown at $T_{\text{sub}} = 580^\circ\text{C}$, which exhibited both 1D and 2D islands, whereas for the 1-p sample grown at the same temperature, the dominant species was $4 \times 4\text{-uc}^2$ SrTiO_3 (see Figure 2a). Figure 2d shows an STM image of a 2-p sample grown at $T_{\text{sub}} = 620^\circ\text{C}$, which exhibited very few $4 \times 4\text{-uc}^2$ SrTiO_3 islands and typically either 1D or 2D islands were formed. Figure 2e shows an STM image of a 3-p sample grown at $T_{\text{sub}} = 580^\circ\text{C}$, and Figure 2f shows

an STM image of 2-p sample grown at $T_{\text{sub}} = 620^\circ\text{C}$. A similar trend can be observed, with the long axes of the 1D islands oriented along either $[100]$ or $[010]$, in roughly equal proportions, as may be expected from the crystal symmetry. This anisotropic growth indicates a strong anisotropy in the diffusion energy barrier of the substrate, which can be clearly distinguished from typical isotropic diffusion of metals on metal substrates [18,19].

The STM images shown in Figure 2 also reveal that the changes in the island growth patterns were related to the substrate surface structures. Figure 3a shows STM images of 1-p sample grown at $T_{\text{sub}} = 620^\circ\text{C}$. We can see a 2D connection between the bright contrast of the two aligned along the two equivalent surface crystallographic directions. Similar structures have been reported for the surface of a 10-*uc*-thick SrTiO_3 homoepitaxial film [25]. An STM image obtained with different tip conditions is shown overlaid in the inset of Figure 3a, for the same area with the same length scale, which reveals 2×2 periodicity. The apparent difference in the patterns of the STM contrasts measured on the same sample surface with an identical periodicity (i.e., 2×2) may be attributed to different contributions of the electronic structures of the tips. This reflects the importance of the local electronic structure of the tip and sample in the STM contrast rather than the sample geometry and emphasizes that care is required in the interpretation of the apparent height in STM images. To identify the symmetry of the local surface electronic structure, we carried out Fourier transform (FT) power spectrum analysis of the image in Figure 3a, as shown in Figure 3e. The bright spots at $(1/2\ 0)$ in the FT power spectrum are indicative of the existence of a (2×2) RC [26] in the substrate surface. Theoretical modeling [14,27,28] and transmission electron microscopy [29] of the SrTiO_3 surface suggest that oxygen vacancies form linear clusters in SrTiO_3 , which may explain the (2×2) RC as pairs of oxygen vacancy clusters.

The bright spots shown in Figure 3a distributed randomly in the 1-p sample; however, similar features were more ordered in the 2-p sample, as shown in Figure 3b. Such order was very rarely observed in the as-prepared substrate surface and the 1-p sample grown at $T_{\text{sub}} = 580^\circ\text{C}$ (see Figure 2a). The apparent height of these spots as determined from the STM data was in the range 0.15 to 0.2 nm, as shown in the profiles in Figure 3d. Theoretical modeling of the SrTiO_3 surface [28] has shown that oxygen vacancies at the SrO layer exhibit high electron density. In our case, we expect that the O vacancy of the subsurface SrO layer may induce a similar change in the local electron density of the TiO_2 layer at next above the vacancy position, which might contribute to the enhanced STM contrast of the

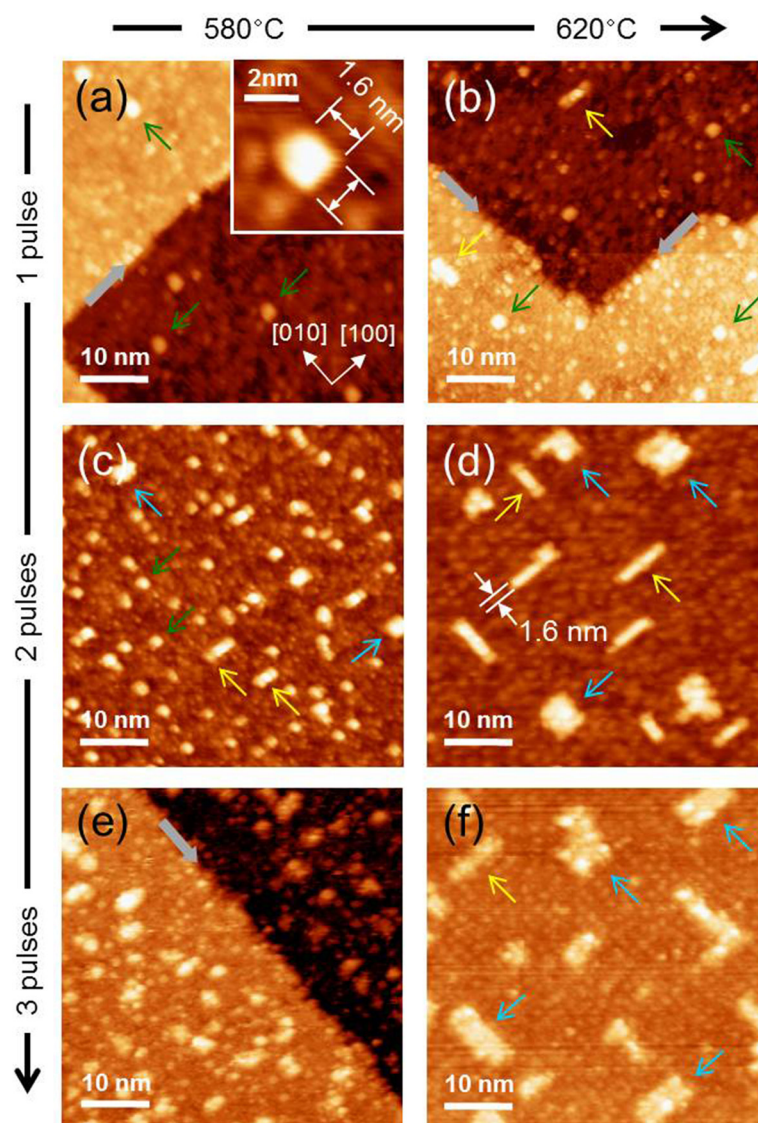


Figure 2 STM images for initial growth patterns in SrTiO_3 homoepitaxy. (a) and (b) $50 \times 50\text{-nm}^2$ STM images of 1-p samples grown at 580°C and 620°C , respectively. (c) and (d) ((e) and (f)) 2-p (3-p) samples grown at 580°C and 620°C , respectively. All STM images were obtained with $V_S = 2.0\text{ V}$ and $I_{\text{set}} = 50\text{ pA}$. The green arrows indicate the smallest islands, which are 1 uc high. The yellow (cyan) arrows indicate 1D (2D) SrTiO_3 islands. The inset of (a) shows a $7 \times 7\text{-nm}^2$ STM image of a SrTiO_3 island, as indicated by the green arrow. The gray arrows in (a), (b), and (e) indicate the substrate monatomic-high step edges.

apparent defects on the surface. Interestingly, we observed that these defects were aligned along the crystal symmetry directions. The separation of these defects was 1.6 nm (approximately 4 uc), as identified from the line profiles shown in Figure 3d. Moreover, a 2D expansion of an array of these defects was observed as the defect density increased, as shown in Figure 3b, c. In the 3-p sample shown in Figure 3c, such arrays of defects fully occupied the surface with 2D $4 \times 4\text{-uc}$ periodicity. This periodicity is also apparent in the FT power spectrum map of the image in Figure 3c, as shown in Figure 3f, where 4-uc periodicity can be observed along the crystal symmetry directions.

Stable configurations of the primary SrTiO_3 islands occurred in parallel with the development of the defect-induced RC formations, and the geometry of these features was related to the crystallographic symmetry of the SrTiO_3 (001) surface. Phark et al. reported [17] the failure of epitaxial growth, together with the absence of notable changes in the surface structure during deposition, for homoepitaxy on a (6×2) RC surface. This supports the possibility of defect-induced surface RC formations, i.e., $4 \times 4\text{-uc}$ periodic arrays of defects, as a prerequisite or precursor that is significant in the activation of nucleation and growth during SrTiO_3

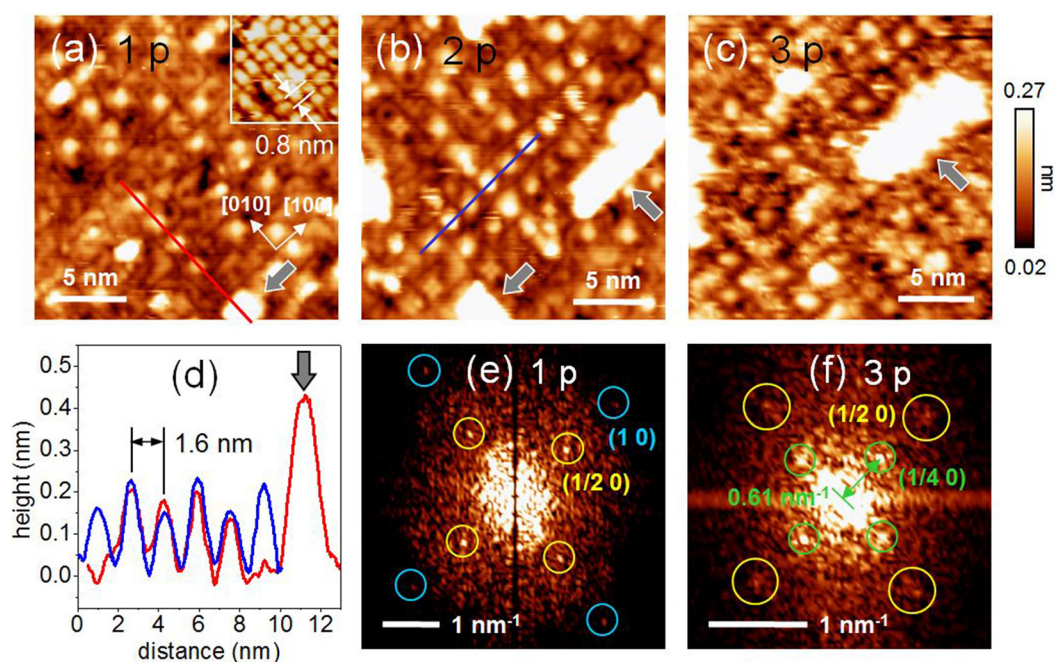


Figure 3 STM images for defect formations in the initial growth stage. (a) to (c) 20 × 20-nm² STM images showing the formation of defects in the substrate surfaces of 1-, 2-, and 3-p samples, respectively. All STM images were obtained with $V_s = 2.0$ V and $I_{set} = 50$ pA. The inset of (a) shows an STM image of the same area with the same length scale that was obtained using a different tip. The gray arrows indicate large white structures, which are 1-uc-high SrTiO₃ islands. The red (blue) curve in (d) shows the STM apparent height profile along the red (blue) line in (a) ((b)). (e) FT power spectrum map of (a). The yellow circles show bright spots in the FT power spectrum at (1/2 0), which are indicative of 2 × 2 RC. (f) FT power spectrum map of (c). The bright spots indicated by the green circles at (1/4 0) correspond to a periodicity of 4 uc along the directions of crystal symmetry.

homoepitaxy. Further theoretical work may expand our understanding of the connection between the surface RC and the initial stages of growth during SrTiO₃ homoepitaxy.

Careful attention was paid to the growth conditions in this study, which enabled us to observe the nucleation of SrTiO₃ islands and the growth of perovskite nanostructures via the addition of SrTiO₃ molecular units. This work makes an important contribution to conventional diffusion/nucleation theory for metal-on-metal epitaxy, extending it to complex oxide systems. Further investigation should be carried out to characterize the minimum nucleation size and the energy E_d to improve our understanding of the differences in the diffusion characteristics of the perovskite-perovskite systems compared to metal-metal epitaxy.

Conclusions

We have investigated the growth of SrTiO₃ islands on SrTiO₃ (001) surface using PLD and *in situ* STM. We found that 4 × 4-uc² islands form as nucleation seeds, which grow along the crystal axes with a width of 4 uc. This result suggests that energetically stable nucleation of SrTiO₃ islands is related to (2 × 2) surface reconstruction, with the formation of 4-uc periodic arrays of

defects. Our observations represent an atomic-scale approach to understand the initial stages of growth of SrTiO₃ and the importance of the energetic stability of SrTiO₃ (001) surface RC via oxygen vacancies in the perovskite crystal.

Abbreviations

FT: fourier transform; ML: monolayer; PLD: pulsed laser deposition; RC: reconstruction; RHEED: reflected high energy electron diffraction; STM: scanning tunneling microscopy; UHV: ultra-high vacuum; uc: unit-cell.

Competing interests

The authors declare that they have no competing interests.

Authors' contributions

SHP and YJC conceived and designed the experiments, prepared samples, and performed STM measurements. SHP analyzed the STM data. Both authors discussed the results and wrote the paper. Both authors have read and approved the final manuscript.

Acknowledgements

SHP acknowledges the support from IBS-R009-D1. YJC acknowledges the support from the National Research Foundation of Korea under Grant No. NRF-2014R1A1A1A1002868.

Author details

¹Center for Correlated Electron Systems, Institute for Basic Science (IBS), Seoul National University, Seoul 151-747, Republic of Korea. ²Department of Physics and Astronomy, Seoul National University, Seoul 151-747, Republic of Korea. ³Department of Physics, University of Seoul, Seoul 130-743, Republic of Korea.

Received: 11 December 2014 Accepted: 6 February 2015

Published online: 26 February 2015

References

1. Tokura Y, Taguchi Y, Okada Y, Fujishima Y, Arima T, Kumagai K, et al. Filling dependence of electronic properties on the verge of metal-Mott-insulator transition in $\text{Sr}_{1-x}\text{La}_x\text{TiO}_3$. *Phys Rev Lett*. 1993;70:2126.
2. Haeni JH, Irvin P, Chang W, Uecker R, Reiche P, Li YL, et al. Room-temperature ferroelectricity in strained SrTiO_3 . *Nature*. 2004;430:758–61.
3. Kim YS, Kim DJ, Kim TH, Noh TW, Choi JS, Park BH, et al. Observation of room-temperature ferroelectricity in tetragonal strontium titanate thin films on SrTiO_3 (001) substrates. *Appl Phys Lett*. 2007;91:042908.
4. Ueno K, Nakamura S, Shimotani H, Ohtomo A, Kimura N, Nojima T, et al. Electric-field-induced superconductivity in an insulator. *Nat Mater*. 2008;7:855–8.
5. Ohtomo A, Hwang HY. A high-mobility electron gas at the $\text{LaAlO}_3/\text{SrTiO}_3$ heterointerface. *Nature*. 2004;427:423–6.
6. Thiel S, Hammerl G, Schmehl A, Schneider CW, Mannhart J. Tunable quasi-two-dimensional electron gases in oxide heterostructures. *Science*. 2006;313:1942–5.
7. Chang YJ, Moreschini L, Bostwick A, Gaines GA, Kim YS, Walter AL, et al. Layer-by-layer evolution of a two-dimensional electron gas near an oxide interface. *Phys Rev Lett*. 2013;111:126401.
8. Brinkman A, Huijben M, van Zalk M, Huijben J, Zeitler U, Maan JC, et al. Magnetic effects at the interface between non-magnetic oxides. *Nat Mater*. 2007;6:493–6.
9. Chang YJ, Kim CH, Phark SH, Kim YS, Yu J, Noh TW. Fundamental thickness limit of itinerant ferromagnetic SrRuO_3 thin films. *Phys Rev Lett*. 2009;103:057201.
10. Reyren N, Thiel S, Caviglia AD, Kourkoutis LF, Hammerl G, Richter C, et al. Superconducting interfaces between insulating oxides. *Science*. 2007;317:1196–9.
11. Caviglia AD, Gariglio S, Reyren N, Jaccard D, Schneider T, Gabay M, et al. Electric field control of the $\text{LaAlO}_3/\text{SrTiO}_3$ interface ground state. *Nature*. 2008;456:624–7.
12. Silly F, Castell MR. Selecting the shape of supported metal nanocrystals: Pd Huts, hexagons, or pyramids on SrTiO_3 (001). *Phys Rev Lett*. 2005;94:046103.
13. Willmott PR, Herger R, Schleputz CM, Martocchia D, Patterson BD. Energetic surface smoothing of complex metal-oxide thin films. *Phys Rev Lett*. 2006;96:176102.
14. Cuong DD, Lee B, Choi KM, Ahn H-S, Han S, Lee J. Oxygen vacancy clustering and electron localization in oxygen-deficient SrTiO_3 : LDA + U study. *Phys Rev Lett*. 2007;98:115503.
15. Castell MR. Scanning tunneling microscopy of reconstructions on the SrTiO_3 (001) surface. *Surf Sci*. 2002;505:1–13.
16. Koster G, Rijnders G, Blank DHA, Rogalla H. Surface morphology determined by (001) single-crystal SrTiO_3 termination. *Physica C Supercond*. 2000;339:215–30.
17. Phark SH, Chang YJ, Noh TW. Selective growth of perovskite oxides on SrTiO_3 (001) by control of surface reconstructions. *Appl Phys Lett*. 2011;98:161908.
18. Bott M, Hohage M, Morgenstern M, Michely T, Comsa G. New approach for determination of diffusion parameters of adatoms. *Phys Rev Lett*. 1996;76:1304.
19. Muller B, Nedelmann L, Fischer B, Brune H, Kern K. Initial stages of Cu epitaxy on $\text{Ni}(100)$: Postnucleation and a well-defined transition in critical island size. *Phys Rev B*. 1996;54:17858.
20. Kawasaki M, Takahashi K, Maeda T, Tsuchiya R, Shinohara M, Ishiyama O, et al. Atomic control of the SrTiO_3 crystal surface. *Science*. 1994;266:1540–2.
21. Erdman N, Poeppelmeier KR, Asta M, Warschkow O, Ellis DE, Marks LD. The structure and chemistry of the TiO_2 -rich surface of SrTiO_3 (001). *Nature*. 2002;419:55–8.
22. Herger R, Willmott PR, Bunk O, Schleputz CM, Patterson BD, Delley B. Surface of strontium titanate. *Phys Rev Lett*. 2007;98:076102.
23. Mao HJ, Song C, Cui B, Wang GY, Xiao LR, Pan F. Room temperature spontaneous exchange bias in $(\text{La}, \text{Sr})\text{MnO}_3/\text{PbZr}_{0.8}\text{Ti}_{0.2}\text{O}_3/(\text{La}, \text{Sr})\text{MnO}_3$ sandwich structure. *J Appl Phys*. 2013;114:043904.
24. Lippmaa M, Nakagawa N, Kawasaki M, Ohashi S, Koinuma H. Growth mode mapping of SrTiO_3 epitaxy. *Appl Phys Lett*. 2000;76:2439–41.
25. Ohsawa T, Iwaya K, Shimizu R, Hashizume T, Hitosugi T. Thickness-dependent local surface electronic structures of homoepitaxial SrTiO_3 thin films. *J Appl Phys*. 2010;108:073710.
26. Silly F, Newell DT, Castell MR. SrTiO_3 (001) reconstructions: the (2×2) to $c(4 \times 4)$ transition. *Surf Sci*. 2006;600:219–23.
27. Hou Z, Terakura K. Defect states induced by oxygen vacancies in cubic SrTiO_3 : First-principles calculations. *J Phys Soc Jpn*. 2010;79:114704.
28. Zhuang HL, Ganesh P, Cooper VR, Xu H, Kent PRC. Understanding the interactions between oxygen vacancies at SrTiO_3 (001) surfaces. *Phys Rev B*. 2014;90:064106.
29. Jia CL, Lentzen M, Urban K. Atomic-resolution imaging of oxygen in perovskite ceramics. *Science*. 2003;299:870–3.

Submit your manuscript to a SpringerOpen[®] journal and benefit from:

- Convenient online submission
- Rigorous peer review
- Immediate publication on acceptance
- Open access: articles freely available online
- High visibility within the field
- Retaining the copyright to your article

Submit your next manuscript at ► springeropen.com